An official publication of the International Society for Energy, Environment and Sustainability (ISEES)

Journal of Energy and Environmental Sustainability

Journal homepage : www.jees.in



Effect of Fuel Injection Spray Angle on NOx and Soot Emission in CI Engine Using Unsteady Flamelet Model

Anil Bhurao Wakale, R Banerjee[1]

Department of Mechanical & Aerospace Engineering, Indian Institute of Technology Hyderabad, Kandi, Sangareddy- 502284, India

ARTICLE INFO

Received : 26 September 2023
Revised : 02 April 2024
Accepted : 15 April 2024

Keywords:
Ketone; 2-Butanone; 4-Methyl-2-Pentanone; Spark-ignition Engine; Super premium gasoline; Engine characteristics

ABSTRACT

Effect of piston wall wetting due to misalignment in fuel injection on NOx and soot emissions were estimated using 3D CFD modelling in a CI engine with compression ratio of 18. Eulerian- Lagrangian approach was used in this study where the time history of fuel spray and atomization was modeled in the Lagrangian framework whereas in-cylinder aerodynamics was modeled by solving the 3D Navier Stokes equation in the Eulerian framework. Turbulence was modeled using k-ε model. A 6-hole fuel injector was used in this work and only 1/6th sector of the engine volume was modeled assuming uniform fuel injection. Combustion was modelled using by using 246 species and 1062 reactions containing skeletal n-dodecane/n-butanol/NOx/Polycyclic Aromatic Hydrocarbon (PAH) combustion mechanism that was previously developed and reported in open literature (Wakale, Banerjee and Banerjee, 2020). Two fuel injection pressures of 800 bars and 1500 bars and three different fuel spray cone angles of 80o, 120o and 159o were modeled. It was found that lower spray cone angle increases the propensity of soot formation at lower injection pressure. However, it was found that soot formation is not significantly affected by wall wetting and higher injection pressure.

© 2024 ISEES, All rights reserved

1. Introduction

Compression ignition (CI) based internal combustion engines (Heywood, 2018) have been in existence for over a century and find applications for a wide range of engineering applications ranging from powering automotive vehicles to auxiliary power units. Due to non-premixed combustion, NOx and soot emissions are of particular concern for CI engines. Diesel fuel is injected at high pressure inside the cylinder before it auto-ignites to power the engines. Due to high compression ratios that is seen in CI engines, fuel may wet piston and cylinder walls depending upon the proximity of these wall to the liquid jet. The spray cone angle of the fuel injectors is designed such that such wall wetting is avoided. However, it is possible that the spray angle can get altered due to fouling in the injector orifices which in turn can alter spray cone angle which in turn can lead to wall wetting. Such wetting can lead to increased emissions and therefore engine performance needs to be evaluated at off-design spray angles.

Cylinder wall wetting and its effects on engine emission has been studied for both spark ignition (SI) and compression ignition (CI) engines. Li *et al.*, (1999), Stanglmaier, Li and Matthews, (1999) studied the effect of wall wetting on unburnt and partially burnt hydrocarbon emissions in gasoline direct ignition (GDI) and port fuel ignition engines. They found that fuel impingement on the exhaust side of the cylinder liner and on piston wall resulted in higher emissions. Chin and Lee, (2002) have numerically studied hydrocarbon emissions in small GDI engines. They also concluded that wall wetting near exhaust port causes the maximum emission due to easy escape of the hydrocarbon vapors from the exhaust. Also, the liquid film becomes increasingly composed of higher hydrocarbons due to early evaporation of the lighter hydrocarbons and this heavier liquid film controls the engine emission due to wall wetting. Malaguti *et al.*, (2009) studied wallwetting under cold engine conditions using numerical simulations. Luijten *et al.*, (2013) used shadowgraph method to visualize wall wetting and film evaporation under different engine operating conditions in GDI engine. Kale and Banerjee, (2021) have demonstrated that piston wall wetting in a GDI engine leads to soot combustion and fuel injection timing and flash boiling of fuel during injection can be used to reduce wall wetting.

Wall wetting is also an issue with CI engines that leads to higher engine emissions. Hulkkonen *et al.*, (2017) studied the effect of diesel and bio-diesel injection late in the engine cycle after the main injection to oxidize particulate matter. This leads to wall wetting and consequently oil dilution leading to engine wear. Bozic *et al.*, (2011) too investigated effect of wall wetting during late fuel injection for particulate filter regeneration when using diesel and palm and soya derived bio-diesel. Woo, Kook and Hawkes, (2016) studied ethanol direct injection based diesel engine operating under gasoline compression ignition mode. They found inlet air temperature affects

*Corresponding Author: *rajabanerjee@mae.iith.ac.in*

© 2024 ISEES, All rights reserved

wall wetting which in turn affects combustion significantly. Yu *et al.*, (2015) studied the effect of spray cone angle on mixture formation and CO/soot emission in an early injection homogeneous charge compression ignition (HCCI) diesel engine. The numerical simulation suggested that wall wetting was the principle cause of these emissions. Boot *et al.*, (2009) proposed the use of uncooled EGR as a means to limit cylinder wall wetting in early direction injection premixed charge compression ignition engines.

Numerical modelling to study in-cylinder combustion is now extensively used to study internal combustion engine performance. Haworth, (2005) provide an excellent review of the various numerical methods used in numerical simulation of in-cylinder combustion. There is an increased trend in using data-driven techniques like Machine Learning that are being used to study andunderstand combustion for various applications due to the relatively fast computation speeds that traditional physics-based models (Raman and Hassanaly, 2019; Aliramezani, Koch and Shahbakhti, 2022). However, such models tend to be more heuristic and require large sample sizes to build reliable models that can be used as digital twin and optimization. Combustion of hydrocarbons consists of several thousand underlying reactions involving thousands of chemical species. The rate kinetics of these reactions span across several orders of magnitude making the system of ODEs solving these reactions very stiff. Therefore, detailed modelling of combustion mechanism along with a 3D Navier Stokes solver along with other physics like turbulence modelling, spray modelling, etc is not practical. Combustion modelling techniques try of reduce this complexity to render combustion simulations practical. Some of the more common combustion modelling techniques that have been used to simulate non-premixed turbulent combustion as typically seen in diesel engines are:

Thickened Flame Model (Butler and O'Rourke, 1977; Cuenot, Shum-Kivan and Blanchard, 2022) – Here the combustion rate parameters are changed such that the reaction zone becomes thick while maintaining the heat release or flame speed. This helps in solving simulating combustion on coarse computational mesh.

Eddy-breakup model (Spalding, 1971; Nicolleau and Mathieu, 1994) – It assumes that the time scale of chemical reaction is very small compared to turbulent mixing and therefore turbulence transport of species becomes the rate controlling parameter. The Eddy Dissipation Model proposed by Magnussen and Hjertager, (1977) is a variant of the EBU model. However, these models have limitations where the reaction kinetics are slow like the NOx mechanism.

In *Conditional Moment Closure (CMC) method* (De Paola *et al.*, 2008; Bolla, Gudmundsson, *et al.*, 2013; Bolla, Wright, *et al.*, 2013; Bolla *et al.*, 2014), conditionally averaged transport equations are considered and the conditioning variables are the ones which have the most significant bearing on the chemical production term. Mixture fraction, which is defined as local mass fraction of the material that originated form the reactant fuel is typically used as the conditioning variable.

Flamelet Models (Peters, 1984; Pitsch, Wan and Peters, 1995; Pitsch, Barths and Peters, 1996; Barths, Antoni and Peters, 1998) view that a turbulent diffusion flame is an ensemble of laminar diffusion flamelets. It assumes that the dominant spatial gradients are in the direction normal to the flame front. The coupling of non-equilibrium combustion chemistry and turbulence reduces the empiricism with limited computational overhead.

PDF Methods (Pope, 1985; Muradoglu *et al.*, 1999) a modelled PDF transport equation, usually by means of a Lagrangian Monte Carlo particle based method. Here the emphasis is the modelling of molecular transport processes instead of the chemical source terms. Modelling is done in Lagrangian framework using deterministic or stochastic approaches to mimic physical mixing effects of turbulent reacting flows.

As seen from above that cylinder wall wetting leads to higher unburned HC emissions. However, most of the work reported are for GDI engines and limited to gross evaluation of the tail pipe emissions. Only limited work on in-cylinder wall wetting in CI engines has been reported in open literature. However, they can become a potential source of emissions in older CI engines where deposits inside the injector orifices may alter the injection pattern in such engines. This work reports a detailed analysis of the effect of spray cone angle on piston wall wetting andsubsequent NOx and soot emissions in a CI engine. Such simulations can be part of robust engine design process and potential source of emissions can be detected in the early phase of engine design. Three different spray cone angle is simulated where the base case is on where the liquid jet is directed deep inside the piston bowl and hence, does not interact with the piton walls. The numerical simulations would present the wall wetting of the piston wall and its evolution with time. Combustion kinetics and turbulence interaction was modeled using unsteady flamelet model and all simulations were performed using Ansys Fluent ver. 18.

2. Mathematical Formulation

Commercially available 3D CFD solver Ansys Fluent v18 was used in this work. The details of the mathematical formulation used is given below:

2.1 Droplet Tracking

Lagrangian framework was used to track the droplet time-history. Droplet acceleration was modeled as,

$$\frac{d\vec{u}_p}{dt} = \frac{18\mu}{\rho_p d_p^2}\frac{C_D Re}{24}\left(\vec{u} - \vec{u}_p\right) \quad (1a)$$

where *Re* number is calculated as,

$$Re = \frac{\rho d_p \left|\vec{u} - \vec{u}_p\right|}{\mu} \quad (1b)$$

And coefficient of drag, C_D is determined as,

$$C_D = a_1 + \frac{a_2}{Re} + \frac{a_3}{Re} \quad (1c)$$

The model constants a_1, a_2 and a_3 are taken from Morsi and Alexander, (1972). Droplet temperature time history was tracked as,

$$m_p c_p \frac{dT_p}{dt} = hA_p\left(T_\infty - T_p\right) + \frac{dm_p}{dt}h_{fg} \quad (2)$$

The convective heat transfer coefficient, h is determined by using the Ranz and Marshall, (1952a, 1952b) correlation. Droplet evaporation rate is determined as,

$$\frac{dm_p}{dt} = k_c\left(\frac{p_{Sat}\left(T_p\right)}{RT_\infty} - C_{i.\infty}\right)A_p M_w \quad (3)$$

The mass transfer coefficient, k_c is determined by using correlation proposed by Ranz and Marshall, (1952a, 1952b). The thermophysical properties of the fuel like specific heat, thermal conductivity, saturation pressure, etc were used estimated using piecewise linear profiles. Blob primary injection model was assumed where the initial droplet of the injected fuel was equal to the injection orifice diameter. Coefficient of discharge (C_D) and coefficient of velocity (C_v) of 0.8 and 0.93 has been assumed, respectively and was used to determine the fuel injection mass flowrate and velocity. Subsequently, the secondary breakup was modeled using KH-RT model proposed by Beale and Reitz, (1999). The model constants for secondary breakup used in this work has been reported previously (Wakale, Banerjee and Banerjee, 2020).

2.2 Continuous Phase

In-cylinder aerodynamics was modeled in the Eulerian framework. The following equations were modeled for the gas phase:

Continuity Eq

$$\frac{\partial \rho}{\partial t} + \dot{\nabla}\cdot\left(\rho\vec{u}\right) = S \quad (4)$$

Where S is the source term added to the continuous phase due to droplet evaporation.

Momentum Eq

$$\frac{\partial\left(\rho\vec{u}\right)}{\partial t} + \nabla\cdot\left(\rho\vec{u}\vec{u}\right) = -\nabla p + \nabla\cdot\left[\mu_{eff}\left(\nabla\vec{u} + \nabla\vec{u}^T\right)\right] + S_m \quad (5)$$

Where S_m is the source term added to the continuous phase momentum equation due to interfacial momentum exchange arising due to drag force.

Energy Eq

$$\frac{\partial(\rho E)}{\partial t} + \nabla \cdot [\vec{u} \cdot (\rho E + p)] = \nabla \cdot \left[k_{eff} \nabla T - \sum_j h_j \vec{J}_j \right] + S_e \quad (6)$$

Where energy, $E = h - \frac{p}{\rho} + \frac{u^2}{2}$, enthalpy of the j^{th} species is given as $h_j = \int_{T_{ref}}^{T} c_{p,j} dT$ and diffusion flux, $\vec{J} = -\left(\rho D_{i,m} + \frac{\mu_t}{Sc_t}\right) \nabla y_i$. S_e is the source term due to heat transfer between the continuous and dispersed phases.

Species Eq

$$\frac{\partial(\rho y_i)}{\partial t} + \nabla \cdot (\rho \vec{u} y_i) = \nabla \cdot \vec{J}_i + S_i \quad (6)$$

The source term of the i^{th} is S_i and

2.3 Combustion Model

Combustion of diesel in a compression ignition engine can be considered as non-premixed turbulent combustion. In this work, flamelet based method has be used because this approach uses reduced or skeletal combustion mechanism and therefore model based empiricism is minimized. On the other hand, it solves two additional convection-diffusion equation and therefore it is computationally not very expensive. Peters, (1984) shown that a turbulent flame front can be represented as an ensemble of multiple laminar diffusion flamelets. By assumingfast reactions, the combustion time scales and turbulent time scales can be separated. Therefore, combustion chemistry is independently computed in the mixture fraction space and are assumed to be not affected by the local turbulent eddies. Mixture fraction is expressed as,

$$f = \frac{Z_i - Z_{i,ox}}{Z_{i,f} - Z_{i,ox}}$$

where, Z_i is the elemental mass fraction of the i^th element, Z_(i,ox) is the elemental mass fraction of the oxidizer and Z_(i,f) is the elemental mass fraction of the fuel. f=1 in the fuel stream and f=0 in the oxidizer stream. Hence, the variation of the mass fraction of the i^th species can be mapped to the mixture fraction. Under the condition when the iso-f surface curvature is not too strong, the gradients in the direction perpendicular to the stoichiometric is dominant and therefore, scalar dissipation rate can be related to the gradient of the mixture fraction as,

$$\chi = 2D|\nabla f|^2$$

Where D is the diffusion coefficient. As χ_st is the scalar dissipation rate at the stoichiometric mixture fraction, f_st, a non-zero value of χ_st indicates non-equilibrium combustion chemistry and value higher than a certain threshold results in local quenching of the flame.

The flamelet is generated by writing the species mass fraction, y_i in the mixture fraction space as,

$$\rho \frac{\partial y_i}{\partial t} = \frac{1}{2} \rho \chi \frac{\partial^2 y_i}{\partial f^2} + S_i$$

Temperature (T) equation is expressed as,

$$\rho \frac{\partial T}{\partial t} = \frac{1}{2} \rho \chi \frac{\partial^2 T}{\partial f^2} - \frac{1}{C_p} \sum_i h_i S_i + \frac{1}{2C_p} \rho \chi \left[\frac{\partial C_p}{\partial f} + \sum_i C_{p,i} \frac{\partial y_i}{\partial f} \right] \frac{\partial T}{\partial f}$$

Instantaneous scalars like species mass fraction, temperature, density, etc are dependent on mixture fraction and scalar dissipation rate at stoichiometric value of mixture fraction, i.e. ϕ=ϕ(f,χ_st). Turbulence-chemistry interaction is modelled by assuming a β-function based probability distribution function with respect to f and δ-function for χ. Turbulence affects the mean flow parameters and is accounted by solving the transport equations of the mean and the second moment of the mixture fraction, respectively as shown below,

$$\frac{\partial(\bar{\rho}\tilde{f})}{\partial t} + \nabla \cdot (\bar{\rho}\tilde{\boldsymbol{u}}\tilde{f}) = \nabla \cdot \left[\left(\frac{\tilde{k}}{C_p} + \frac{\mu_t}{\sigma_t} \right) \nabla \tilde{f} \right] + S_m$$

and

$$\frac{\partial}{\partial t}(\bar{\rho}\widetilde{f''^2}) + \nabla \cdot (\bar{\rho}\tilde{\boldsymbol{u}}\widetilde{f''^2}) = \nabla \cdot \left[\left(\frac{\tilde{k}}{C_p} + \frac{\mu_t}{\sigma_t} \right) \nabla \widetilde{f''^2} \right] + C_g \mu_t \cdot (\nabla \tilde{f}) - C_d \bar{\rho} \frac{\tilde{\varepsilon}}{\tilde{k}} \widetilde{f''^2}$$

Model constant for σ_t , C_g and C_d were taken to be 0.85, 2.86 and 2.0, respectively.

In the present work, Mix246 combustion mechanism was used which is a 246 species and 1062 reaction mechanism. Wakale, Banerjee and Banerjee, (2020) had previously reported the details of this mechanism along with validation of the combustion kinetics and its performance for turbulent spray combustion application within a unsteady flamelet framework. This mechanism consists of a base 203 species and 703 reactions *n*-butanol/*n*-dodecane reaction mechanism. NOx mechanism adopted from GRI-Mech 3.0 (Smith *et al.*, 1999) and a reduced PAH mechanism consisting of 20 species and 124 reactions proposed by Slavinskaya *et al.*, (2012) was added to the base mechanism. PAH profile is taken as a surrogate for soot. Validation of this mechanism using data from ignition delay timings and species profile from flames and Jet Stirred Reactor experiments have been reported by Wakale, Banerjee and Banerjee, (2020). The mechanismshowed a good agreement with reference data and was able to simulated CI engine like combustion conditions.

3. Results & Discussion

Table 1 gives the specifications of the CI engine and the fuel injection parameters that were used in this work. Diesel is a complex hydrocarbon mixture consisting of hundreds of different hydrocarbons and therefore simpler hydrocarbons like *n*-heptane (Som and Aggarwal, 2010; Som *et al.*, 2011), *n*-decane (Jahangirian *et al.*, 2012) and *n*-dodecane (Jahangirian *et al.*, 2012) have been used in literature as surrogates to simulate diesel fuel combustion. In this work *n*-dodecane has been used as it is also able to simulate the higher hydrocarbon combustion chemistry and its properties is given in Table 2. As mentioned above, the combustion kinetics is implemented through Mix246.

Table 1: CI Engine and Fuel Injection Parameters

Engine Specifications	
Displaced volume	693.7cc
Stroke	100 mm
Bore	94 mm
Connecting rod length	235 mm
Compression ratio	18:1
Inlet valve close (IVC)	159° BTDC
Exhaust valve open (EVO)	155° ATDC
Injection Parameters	
Fuel injection velocity	418 m/s @ FIP=800 bar, 579 m/s @ FIP=1500 bar
Fuel injection mass flow rate	3.05 g/s @ FIP=800 bar, 4.23 g/s @ FIP=1500 bar
Fuel temperature	363 K
Start of injection	9° BTDC
End of injection	1.56° BTDC
Spray cone angle	80°, 120°, 159°
Orifice diameter	0.12 mm

Table 2 Fuel Properties of *n*-dodecane

Properties	Values
Density (kg/m^3)	749.5
Lower heating value (MJ/kg)	44.15
Boiling point (K)	489.3
Latent heat (kJ/kg)	310.66

Table 3: Definitions of Emissions

Polycyclic Aromatic Hydrocarbons (PAH)	Benzene (A1)
	Naphthalene (A2)
	Acenapthalene (A2R5)
	Phenanthrene (A3)
	Pyrene (A4)
Nitrogen Oxides (NOx)	Nitrous Oxide (N_2O)
	Nitric Oxide (NO)
	Nitrogen Dioxide (NO_2)
uHC	Methane (CH_4)
	Ethane (C_2H_6)
	Propane (C_3H_{10})

3.1 Geometry & Mesh

Fig 1 (a) shows the engine geometry and mesh. A 60° sector in-cylinder volume was modelled because a six-hole fuel injector was simulated and therefore the azimuthal angle between two adjacent orifice hole is 60°. A previously reported experimental study by this group Wakale, Banerjee and

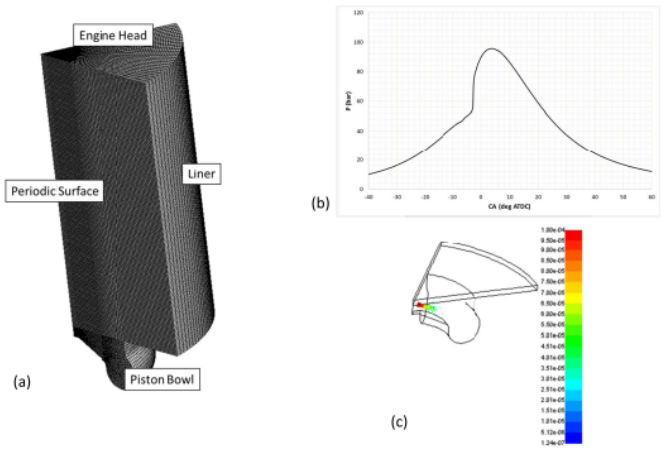


Fig 1: 60° sector engine geometry and mesh at 159° BTDC

Banerjee, (2018) had used a 6-hole injector and therefore the same injector characteristics has been in the present work also. Therefore, a 6-hole injector configuration has been taken in subsequent numerical research work. The cylinder geometry was assumed to be axisymmetric. Therefore, a 60° sector with an injector located at the center of this sector representing 1/6th of the engine cylinder volume was considered. Using sectorial cylinder geometry for studying in-cylinder geometry is common in open literature (Kodavasal *et al.*, 2015; Zhang *et al.*, 2016; Perini *et al.*, 2019) as it is computationally less expensive.

The side wall of this sector was assumed to be periodic and therefore the full 360° geometry can be reconstructed by rotation of this sector six times. The current study was performed during the closed cycle of the compression and power strokes, i.e. between IVC and EVO events. The number of mesh elements at IVC was approximately 401,000 that reduces to approximately 130,000 at TDC. The average mesh size at the beginning of the simulations were approximately 0.6 mm. The selection of the mesh size was based on a detailed analysis of the effect of mesh size on various combustion parameters that has been reported previously (Wakale, Banerjee and Banerjee, 2020). In that study the effect of mesh size on liquid and vapor penetration lengths under non- reacting ECN Spray A condition was reported. It was shown that 0.6 mm mesh gave a good agreement with the experimental data. Furthermore, ignition delay under reacting ECN Spray A condition gave a reasonably good agreement with experimental ignition delay values. Lastly, Grid Convergence Index (GCI) proposed by Celik *et al.*, (2008) was performed on this mesh and it was determined that numerical uncertainty due to mesh was approximately 14.01%. As all sub- models like spray breakup-up model, combustion kinetics, unsteady flamelet based non-premixed turbulent combustion model and modelling parameters like fuel composition and injection pressure of the present study are same as the previous work, it was deemed appropriate that 0.6mm would predict combustion characteristics with the same fidelity as the previous work. The walls were assumed to be adiabatic and the air was quiescent at TDC.

3.2 Base Case

A Base case where the fuel injection pressure (FIP) was 800 bar and the included spray cone angle of 120° was considered the base case in this work. The rest of the parameters were maintained as given in Table 1. The □ □ curve from this case is shown in Fig 1 (b). The peak pressure was approximately 95 bar and the ignition delay was approximately 6.3° crank angles. The polytropic index during the compression stroke was 1.38 and that for the expansion stroke was 1.19. Fig 1 (c) shows the trace of the injected fuel and it can be noticed that the fuel enters the deep pocket of the piston bowl without interacting with the piston walls. The fuel is completely evaporated before reaching the piston walls.

Fig 2 (a) shows the in-cylinder temperature during the expansion stroke. It can be noticed that the flame travels towards the depth of the piston bowl. As was explained earlier (Wakale, Banerjee and Banerjee, 2020), the liquid fuel initially evaporates which is then followed by a pyrolytic breakdown of the hydrocarbon due to the high ambient pressure and temperature. Subsequently, these fragmented hydrocarbons rapidly oxidize to form carbon monoxide indicating onset of combustion. Hence, the in-cylinder peak

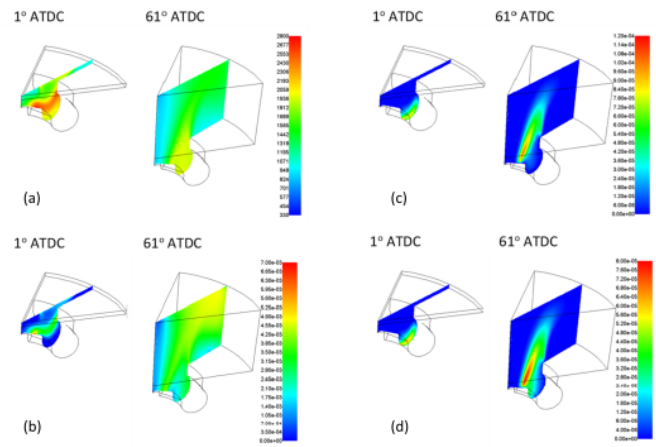


Fig 2: (a) P-□ curve and (b) Droplet Diameter Profile of Injected Fuel

temperature follows the path traced by the fuel as sufficient fuel vapor is required for the onset of combustion. Vigorous combustion due to the conversion of CO to CO_2 leads to the formation of hot combustion gas products that occupy a significant portion of the piston bowl. As the piston moves away from the top dead centre (TDC), the combustion products begin to cool down. NOx profile seen in Fig 2 (b) is similar to the temperature profile because NOx formation is dominated by thermal NOx.

Fig 2 (c) and (d) shows the temporal evolution of unburnt hydrocarbon (uHC) and PAH mass fractions. As mentioned before, PAH is taken as surrogate for soot. Both uHC and soot profilesare very similar. As explained by Wakale, Banerjee and Banerjee, (2020), soot formation is dominated in the regions of the flame where the temperatures are lower than the peak temperature. For this reason, soot is formed either near the region where the flame interacts with the liquid droplets in the rear of the flame or just ahead of the flame. The peak mass fraction of soot reduced by two orders of magnitude when the piston moved from TDC to 21° ATDC. The mass fraction profile of uHC mirrors the soot profile. Initial breakdown of the fuel creates large amount of smaller hydrocarbons due to pyrolysis. However, these hydrocarbons quickly get oxidized leaving a much smaller amount as residual. It seems that this residual uHC is contributing to the formation of soot and therefore the two profiles look very similar. Here again, the peak uHC mass fraction reduced by two orders of magnitude when the piston moved from TDC to 21°ATDC during the expansion stroke.

Fig 3 shows the crank resolved evolution of the soot, uHC and NOx. These values are mass integrals over the entire cylinder volume and are defined as ∫_V□ ϕρdV, where ϕ is the mass fraction of either soot, uHC or NOx. The integral values are normalized by the gross engine power. Gross engine power is determined from the gross work done per cycle which is obtained by performing a numerical integration of pdV from IVC to EVO and it comes out to be 1.51 kW for the base case. uHC formed immediately after the start of fuel injection and rapidly increased and peaked near TDC. The peak value was approximately $60´10^{-6}$ g/kW after which it subsequently reduced rapidly during the mixing-controlled combustion phase of the engine. The uHC value became almost constant by approximately 60°ATDC, and was less than $1´10^{-6}$ g/kW near EVO. As mentioned before, the uHC and soot profiles are very close to each other. In this figure too, it can be seen that the in-cylinder soot value peaked near TDC and subsequently decreased rapidlydue to post combustion oxidation and goes below $1´10^{-6}$ g/kW near EVO. The only difference here is that soot formation begins after a bit of lag compared to

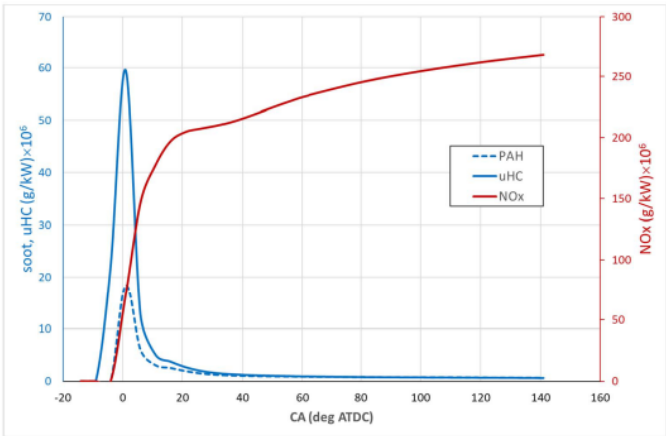


Fig 3: (a) Temperature and (b) NOx Profile During Expansion Stroke

uHC formation and this lag compares with ignition delay, which indicates that liquid droplet and flame interaction triggers formation of PAH, which was also observed previously (Wakale, Banerjee and Banerjee, 2020). On the other hand, NOx formation also started after ignition delay and increased rapidly. The primary route of NOx formation is through the thermal route. As explained by the Zeldovich mechanism, NO, which is the primary constituent of NOx emission is thermally activated through the following elementary reactions

$$\square O + N_2 \rightleftharpoons NO + \square N \qquad \text{R-1}$$

$$\square N + O_2 \rightleftharpoons NO + \square O \qquad \text{R-2}$$

$$\square N + OH \rightleftharpoons NO + \square H \qquad \text{R-3}$$

R-1 is the rate determining step as it has a high activation energy and therefore becomes active only at elevated temperatures. As is seen in Fig 5, there is a rapid rise in NOx formation after the start of combustion, which continues till about 20 deg ATDC. This is the active combustion phase with very high temperatures as seen from the contour plots at 1 °and 21°ATDC of Fig 3(a). At later times, the in-cylinder temperature dropped resulting in a rapid drop in the NO generation kinetics. Hence, NOx formation reduced at the later crank angles of the expansion stroke and therefore, its rate if increase is at much slower pace and the value of NOx is a little above $250'10^{-6}$ g/kW at EVO.

3.3 Parametric Study

A parametric study was performed to see the effect of spray cone angle to emissions. Three different spray angle: 80°, 120° and 159° was simulated at two different fuel injection pressures of 800 bar and 1500 bar. The choice of these spray angles were dictated by the fact that the fuel jet is directed towards the inner depth of the piston bowl at 120° and as shown from the base case simulation, the liquid jet does not interact with the piston walls. On the other hand, it was expected that when the included spray angle is 80°, the liquid jet would impinge on the near piston wall causing wall wetting. Likewise, it was expected that the liquid jet may impinge on the piston outer wall when spray cone angle is increased to 159°. In all these cases, a higher FIP was expected

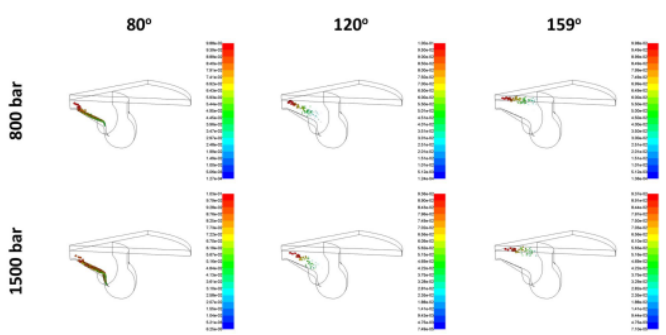


Fig 4: (a) uHC and (b) Soot Profile During Expansion Stroke

to give a stronger liquid jet/wall interaction due to higher momentum of the liquid jet. However, higher FIP improves the atomization of the spray which in turn increases droplet evaporation rate and consequently improved combustion efficiency was expected. As the start and end of fuel injection is same for both the FIPs, the total mass of fuel injected was 3.6 µg when FIP=800 bar and was 5µg when FIP=1500 bar. cone angles. As it is clearly evident form the figure that the spray impinges on the inner piston wall when the cone angle is 80°. The liquid forms a film and it drips downwards towards the inner depths of the piston bowl. Even for the case of 120°, the liquid jet is fairly close towards the inside piston wall and in-cylinder aerodynamics can drift some of the droplets towards the wall. On the other hand, the 159°case is clearly away from all the cylinder and piston walls. Even though it was initially expected that the liquid jet may interact with the piston far wall, it is clearly seen from the figure that this is not happening because the liquid jet is evaporating completely before it reaches close to the walls for both FIPs. It is also evident from the figure that the droplet size is smaller from the 1500 bar case. The minimum droplet size from the 1500 bar case was $7.1'10^{-5}$ mm whereas it was $1.36'10^{-4}$ mm from the 800 bar case. Droplet evaporation is higher for thesmaller droplets. Moreover, higher FIP enhances the propensity of formation of a more homogeneous vapor-air mixture due to higher air entrainment, which improves the overall combustion efficiency.

Fig 5 shows the temperature and emissions at EVO from these two FIPs. The emissions are normalized by the gross power generated between IVC and EVO. Gross power is 1.51 kW when FIP=800 bar and is 2.04 kW when FIP=1500 bar. The exhaust temperature at EVO is estimated by volume averaging the temperature over the entire cylinder volume as defined by the formula, $\frac{1}{V}\int_V TdV$. It is seen that exhaust temperature was consistently higher for the case when FIP=1500 bar compared to the 800 bar case. This is because, a higher amount of fuel is injected when FIP=1500 bar. Additionally, fuel atomization improves at higher injection pressure leading to better combustion efficiency. The average exhaust temperature does not vary significantly with spray cone angle with a marginal drop in temperature when the cone angle is 159°. As expected, NOx emission was higher for FIP=1500 bar which is consistent with higher exhaust gas temperature at EVO. As thermal NOx dominates, higher in-cylinder temperatures will result in higher NOx emission. NOx emission was lowest for 80°spray angle case at FIP=800 bar. This may be because the spray impinges on the piston inner

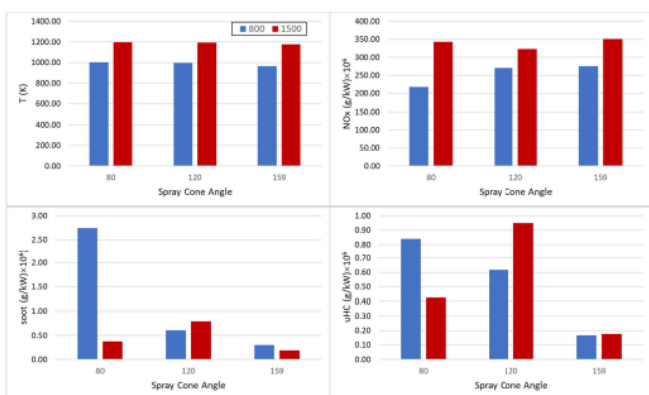


Fig 5: Crank Resolved History of in-Cylinder Evolution of Soot, uHC and NOx

wall and forms a liquid film. This liquid film is still seen at 26° ATDC indicating slow fuel evaporation. As this fuel is not participating in combustion process, the resultant NOx is lower. However, the same was not seen when FIP is increased to 1500 bar. This might be because droplet atomization improves at higher FIP and the smaller droplets evaporates quickly even after impinging on the piston walls.

Soot emission is highest for 80°spray angle case at FIP=800 bar. On the other hand, the soot emission for FIP=1500 bar case with the same spray angle is significantly lower. The largedifference observed in the soot emission between the two FIPs can be explained due to the higher liquid film deposit on the piston wall when FIP=800 bar. This is seen in Fig 6. Luo *et al.*, (2014) has shown that when there is strong two-way coupling when liquid fuel and

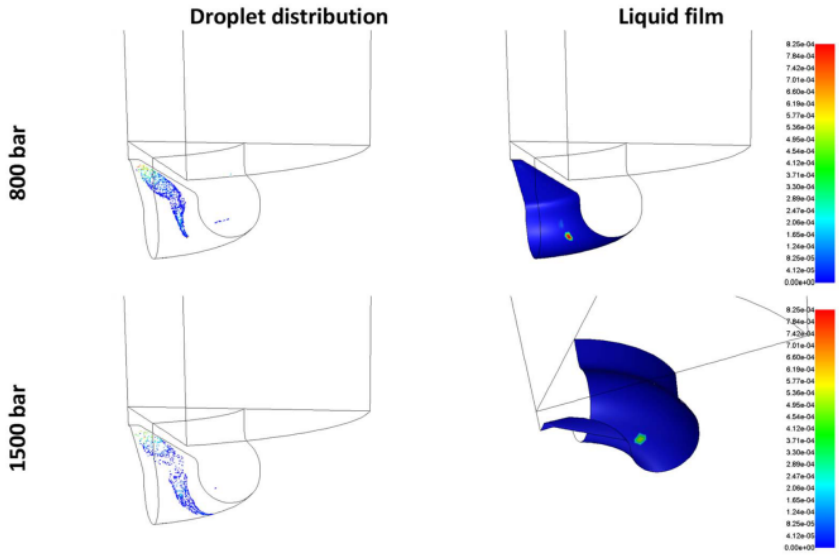


Fig 6: Comparison of Spray Pattern at □ =-4^o ATDC. The droplet size is given in mm

flame interact. Combustion enhances the local heat transfer which in turn increases the fuel evaporation that leads to local temperature drop due to evaporative cooling. This results in a locally fuel rich zone where n-dodecane undergoes thermally induced pyrolytic cracking leading to the formation of lower hydrocarbons like CH_4, C_2H_2, C_4H_4, etc. PAH, which is considered as the surrogate for soot in study, is primarily formed through the Hydrogen-Abstraction-C_2H_2 -Addition and propargyl radical (C_3H_3) recombination pathways. Hence local availability of these hydrocarbons and their conversion to PAH dictates the formation of soot. Unreacted hydrocarbons that do not convert to PAH contribute to uHC. Liquid film is thicker when FIP=800 bar as compared to the case where FIP=1500 bar. Therefore, there is a larger availability of fuel that can get converted to PAH when FIP=800 bars. On the other hand, at higher FIP, film deposition was lower resulting in reduced evaporative cooling. This favors production of uHC through pyrolysis without further conversion to PAH. This explains the significant drop in soot emission when FIP=1500 bar as compared to FIP=800 bar for 80° spray cone angle case even though spray impinges on the piston wall for both the FIPs. The overall soot production for 1500 bar case was less by one order of magnitude compared to 800 bar case. However, the difference in uHC was much smaller.

For the remaining spray angle cases, the soot production from both the FIPs was comparable, with soot for 1500 bar case was marginally higher when spray angle is 120° whereas it was less for 159° spray angle case. These variations might be due to the in-cylinder aerodynamics and local temperature inhomogeneity. The terminal values of uHC were comparable to soot valuesexcept for the case of 800 bar FIP and spray angle of 80°. Unlike the case of soot production where it was an order higher, uHc value for this case was approximately twice when compared with the 1500 bar case for the same spray cone angle. Relatively lower values indicates that uHC components oxidizes faster compared to soot components. This is expected because PAH consists of stable double bonds which would take more energy to break and decompose.

Fig 6 also shows the droplet distribution on the inner piston wall from the two FIP cases where the spray cone angle is 80°. These images are at EVO and therefore at the end of the simulations. As can be seen from the figure, droplets are still present at this crank angle which increases the propensity of the remanent injected fuel to mix with the engine lubricating oil causing oil dilution which have been reported elsewhere (Hulkkonen *et al.*, 2017). As discussed previously, a small region of the piston wall shows formation of liquid film which contributes to high soot emission levels as seen in Fig 5. This film thickness is higher for 800 bar case which is supported by the higher soot emission for this case. Overall, among all the cases simulated in this case, soot emission is highest when FIP=800 bar and spray cone angle is 80°.

4. Conclusion

The current work reports soot, unburnt hydrocarbon and NOx emissions from a diesel engine using 3D numerical modelling. Eulerian-Lagrangian framework was used to simulate turbulent droplet combustion. Unsteady flamelet combustion coupled with a combustion mechanism consisting of 246 species 1062 reactions was used to model combustion. Some of the major conclusions from this work are:

- Propensity of liquid jet impingement on piston inner wall increases when the spray cone angle decreases, which in turn can increase soot emissions, particularly for lower FIPs due to larger droplet size after atomization.
- Consequently, larger spray angle should be favored. In the cases simulated in this work, soot and uHC emissions were lowest when the included spray angle was 159°.
- Injecting within the depths of the piston bowl may be avoided because in-cylinder aerodynamics may cause local spray and wall interaction leading to higher soot emissions.
- NOx emission is only marginally affected by piston wall wetting.

Ethics Approvals

No ethics approvals were taken as this is not applicable to this work.

Consent for publication

All authors have seen this paper and agree with the results and conclusions made in this paper. The authors have given their consent to publish this work in JEES.

Competing interests

Authors declare that they do not have any personal or financial conflicts of interest related to the work reported here.

Funding

The authors would like to acknowledge the financial support by Ministry of Education, Government of India to fund the doctoral research of Dr Anil Bhurao Wakale.

Authors' contributions

Anil B Wakale: Methodology, Software, Validation, Formal analysis, Investigation, Data curation, Writing, Visualization. R Banerjee: Conceptualization, Methodology, Resources, Writing, Supervision.

References

1. Aliramezani, M., Koch, C.R. and Shahbakhti, M. (2022) 'Modeling, diagnostics, optimization, and control of internal combustion engines via modern machine learning techniques: A review and future directions', *Progress in Energy and*

Combustion Science, 88.

2. Barths, H., Antoni, C. and Peters, N. (1998) 'Three-dimensional simulation of pollutant formation in a di diesel engine using multiple interactive flamelets', *982459 SAE Technical Papers* [Preprint]. Available at: https://doi.org/10.4271/982459.
3. Beale, J.C. and Reitz, R.D. (1999) 'Modeling spray atomization with the Kelvin- Helmholtz/Rayleigh-Taylor hybrid model', *Atomization and Sprays*, 9, pp. 623–650.
4. Bolla, M., Gudmundsson, T., *et al.* (2013) 'Simulations of diesel sprays using the conditional moment closure model', *SAE International Journal of Engines*, 6, pp. 1249–1261.
5. Bolla, M., Wright, Y.M., *et al.* (2013) 'Soot formation modeling of n-heptane sprays under diesel engine conditions using the conditional moment closure approach', *Combustion Science and Technology*, 185, pp. 766–793.
6. Bolla, M. *et al.* (2014) 'Modelling of soot formation in a heavy-duty diesel engine with conditional moment closure', *Fuel*, 117(PART A), pp. 309–325.
7. Boot, M.D. *et al.* (2009) 'Uncooled EGR as a means of limiting wall-wetting under early direct injection conditions', *2009-01-0665 SAE Technical Papers* [Preprint].Bozic, G. *et al.* (2011) 'Optical investigation into wall wetting from late-cycle post-injections used for diesel particulate filter regeneration', *Journal of Engineering for Gas Turbines and Power*, 133(9).
8. Butler, T.D. and O'Rourke, P.J. (1977) 'A numerical method for two dimensional unsteady reacting flows', *Symposium (International) on Combustion*, 16(1), pp. 1503–1515. Available at: https://doi.org/10.1016/S0082-0784(77)80432-3.
9. Celik, I.B. *et al.* (2008) 'Procedure for estimation and reporting of uncertainty due to discretization in CFD applications', *Journal of Fluids Engineering, Transactions of the ASME*, 130(7), pp. 780011–780014.
10. Chin, S.T. and Lee, C.-F.F. (2002) 'Numerical investigation of the effect of wall wetting on hydrocarbon emissions in engines', *Proceedings of the Combustion Institute*, 29(1), pp. 767–773. Cuenot, B., Shum-Kivan, F. and Blanchard, S. (2022) 'The thickened flame approach for non- premixed combustion: Principles and implications for turbulent combustion modeling', *Combustion and Flame*, 239, p. 111702.
11. Haworth, D.C. (2005) 'A review of turbulent combustion modeling for multidimensional in- cylinder CFD', *2005-01-0993 SAE Technical Papers* [Preprint].
12. Heywood, J.B. (2018) *Internal combustion engine fundamentals*. McGraw-Hill Education. Hulkkonen, T. *et al.* (2017) 'Late post-injection of biofuel blends in an optical diesel engine: Experimental and theoretical discussion on the inevitable wall-wetting effects on oil dilution', *International Journal of Engine Research*, 18(7), pp. 645–656.
13. Jahangirian, S. *et al.* (2012) 'A detailed experimental and kinetic modeling study of n-decane oxidation at elevated pressures', *Combustion and Flame*, 159, pp. 30–43.Kale, R. and Banerjee, R. (2021) 'Optical investigation of flash boiling and its effect on in-cylinder combustion for butanol isomers and iso-octane', *International Journal of Engine Research*, 25, pp. 1565–1578.
14. Kodavasal, J. *et al.* (2015) 'Computational fluid dynamics simulation of gasoline compression ignition', *Journal of Energy Resources Technology, Transactions of the ASME*, 137(3).
15. Li, J. *et al.* (1999) 'Further experiments on the effects of in-cylinder wall wetting on HC emissions from direct injection gasoline engines', *1999-01-3661 SAE Technical Papers* [Preprint].
16. Luijten, B. *et al.* (2013) 'Experimental investigation of in-cylinder wall wetting in GDI engines using a shadowgraphy method', *2013-01-1604 SAE Technical Papers*, 2.
17. Luo, Z. *et al.* (2014) 'Development and validation of an n-dodecane skeletal mechanism for spray combustion applications', *Combustion Theory and Modelling*, 18(2), pp. 187–203.
18. Magnussen, B.F. and Hjertager, B.H. (1977) 'On mathematical modeling of turbulent combustion with special emphasis on soot formation and combustion', *Symposium (International) on Combustion*, 16, pp. 719–729.
19. Malaguti, S. *et al.* (2009) 'CFD investigation of wall wetting in a GDI engine under low temperature cranking operations', *2009-01-0704 SAE Technical Papers* [Preprint].
20. Morsi, S.A. and Alexander, A.J. (1972) 'An investigation of particle trajectories in two-phase flow systems', *Journal of Fluid Mechanics*, 55, pp. 193–208.
21. Muradoglu, M. *et al.* (1999) 'A Consistent Hybrid Finite-Volume/Particle Method for the PDF Equations of Turbulent Reactive Flows', *Journal of Computational Physics*, 154, pp. 342–371.
22. Nicolleau, F. and Mathieu, J. (1994) 'Eddy break-up model and fractal theory: comparisons with experiments', *International Journal of Heat and Mass Transfer*, 37, pp. 2925–2933.De Paola, G. *et al.* (2008) 'Diesel engine simulations with multi-dimensional conditional moment closure', *Combustion Science and Technology*, 180, pp. 883–899.
23. Perini, F. *et al.* (2019) 'Limitations of sector mesh geometry and initial conditions to model flow and mixture formation in direct-injection diesel engines', in *SAE Technical Papers*.
24. Peters, N. (1984) 'Laminar diffusion flamelet models in non-premixed turbulent combustion', *Progress in Energy and Combustion Science*, 10, pp. 319–339.
25. Pitsch, H., Barths, H. and Peters, N. (1996) 'Three-dimensional modeling of NOx and soot formation in DI-diesel engines using detailed chemistry based on the interactive flamelet approach', *962057 SAE Technical Papers* [Preprint].
26. Pitsch, H., Wan, Y.P. and Peters, N. (1995) 'Numerical investigation of soot formation and oxidation under diesel engine conditions', *952357 SAE Technical Papers* [Preprint].
27. Pope, S.B. (1985) 'PDF methods for turbulent reactive flows', *Progress in Energy and Combustion Science*, 11, pp. 119–192.
28. Raman, V. and Hassanaly, M. (2019) 'Emerging trends in numerical simulations of combustion systems', *Proceedings of the Combustion Institute*, 37(2), pp. 2073–2089.
29. Ranz, W.E. and Marshall, W.R. (1952a) 'Evaporation from Drops, Part I', *Chemical Engineering Progress*, 48, pp. 141–146.
30. Ranz, W.E. and Marshall, W.R. (1952b) 'Evaporation from Drops, Part II', *Chemical Engineering Progress*, 48, pp. 173–180.
31. Slavinskaya, N.A. *et al.* (2012) 'Detailed numerical modeling of PAH formation and growth in non- premixed ethylene and ethane flames', *Combustion and Flame*, 159(3), pp. 979–995.
32. Smith, G.P. *et al.* (1999) *GRI-MECH 3.0*, http://www.me.berkeley.edu/gri_mech/.Som, S. *et al.* (2011) 'Effect of nozzle orifice geometry on spray, combustion, and emission characteristics under diesel engine conditions', *Fuel*, 90, pp. 1267–1276.
33. Som, S. and Aggarwal, S.K. (2010) 'Effects of primary breakup modeling on spray and combustion characteristics of compression ignition engines', *Combustion and Flame*, 157, pp. 1179–1193.
34. Spalding, D.B. (1971) 'Mixing and chemical reaction in steady confined turbulent flames', *Symposium (International) on Combustion*, 13, pp. 649–657.
35. Stanglmaier, R.H., Li, J. and Matthews, R.D. (1999) 'The effect of in-cylinder wall wetting location on the HC emissions from SI engines', *1999-01-0502 SAE Technical Papers* [Preprint].
36. Wakale, A.B., Banerjee, S. and Banerjee, R. (2018) 'Experimental and chemical kinetic study of the impact of n-butanol blending on the gross engine performance of a CRDI engine', *Energy Conversion and Management*, 178, pp. 400–414.
37. Wakale, A.B., Banerjee, S. and Banerjee, R. (2020) 'Estimation of NOx and soot emission from a constant volume n-butanol/n-dodecane blended spray using unsteady flamelet model based on n-dodecane/n-butanol/NOx/PAH chemistry', *Journal of the Energy Institute*, 93(5), pp. 1868– 1882.
38. Woo, C., Kook, S. and Hawkes, E.R. (2016) 'Effect of intake air temperature and common-rail pressure on ethanol combustion in a single-cylinder light-duty diesel engine', *Fuel*, 180, pp. 9–19. Yu, H. *et al.* (2015) 'Numerical investigation of the effect of spray cone angle on mixture formation and CO/soot emissions in an early injection HCCI diesel engine', *2015-01-1070 SAE Technical Paper* [Preprint].Zhang, S. *et al.* (2016) 'A semi-detailed chemical kinetic mechanism of acetone-butanol-ethanol (ABE) and diesel blends for combustion simulations', *SAE International Journal of Engines*, 9(1), pp. 631–640.